361

Developments and applications of a modified wall function for boundary layer flow simulations

Jian Zhang[*1,2], Qingshan Yang[1] and Q.S. Li[2]

[1]*School of Civil Engineering, Beijing Jiaotong University, Beijing, China*
[2]*Department of Civil and Architectural Engineering, City University of Hong Kong, Hong Kong*

Abstract. Wall functions have been widely used in computational fluid dynamics (CFD) simulations and can save significant computational costs compared to other near-wall flow treatment strategies. However, most of the existing wall functions were based on the asymptotic characteristics of near-wall flow quantities, which are inapplicable in complex and non-equilibrium flows. A modified wall function is thus derived in this study based on flow over a plate at zero-pressure gradient, instead of on the basis of asymptotic formulations. Turbulent kinetic energy generation (G_P), dissipation rate (ε) and shear stress (τ_ω) are composed together as the near-wall expressions. Performances of the modified wall function combined with the nonlinear realizable k-ε turbulence model are investigated in homogeneous equilibrium atmosphere boundary layer (ABL) and flow around a 6 m cube. The computational results and associated comparisons to available full-scale measurements show a clear improvement over the standard wall function, especially in reproducing the boundary layer flow. It is demonstrated through the two case studies that the modified wall function is indeed adaptive and can yield accurate prediction results, in spite of its simplicity.

Keywords: wall function; k-ε model; computational fluid dynamics (CFD); atmosphere boundary layer; bluff body

1. Introduction

Computational Fluid Dynamics (CFD) is being widely used for industrial applications. CFD method is well known for its simplicity, strong robustness and good computational economy. It is well suited to simulate atmospheric boundary layer flows.

Numerical simulation of the wind effects on buildings and structures brings several challenges to the applications of CFD to wind engineering. Firstly, computation of flows around buildings and structures requires considering the characteristics of Atmospheric Boundary Layer (ABL). This directly poses difficulties of extracting appropriate boundary conditions, especially at inflow position, for CFD modeling. Secondly, flows around buildings and structures are highly complex.

It is associated with the flows over bluff bodies, where exits separation, reattachment and recirculating regions. The major challenge lies in turbulence modeling with strong anisotropy. Thirdly, topography of configurations is usually complex. Especially in urban areas, closely

---

∗Corresponding author, Dr., E-mail: zjbjtu@gmail.com

located building groups are commonplace, with different geometrical shapes, heights and orientations. Great difficulties are usually encountered when choosing the mesh discretization plans.

Inflow profiles and near-wall flow treatments for CFD simulation, reflecting the characteristics and structures of ABL, should be dealt with properly. These boundary conditions are significantly affected by several factors, such as wall roughness elements, kinematic blocking on the normal fluctuations, the large gradients in mean velocity near wall and flow separation etc. Following the above discussions, the objective of this paper is to propose and validate an extension to the standard wall function method that takes the incident flow profiles and rough wall effects into consideration. And the modified wall function is linked to the two-equation turbulence model. The flow test cases chosen in this study are horizontally homogenous ABL over rough surfaces and flows over a 6 m cube. These case studies focus on the validation of the modified wall function rather than turbulence models. And hereby the results presented and discussed in this paper are all obtained with the realizable k-ε model.

2. Wall function method

With respect to the near-wall treatment strategies, there are three different categories of turbulence modelling methods. The first category is the low Reynolds number (LRN) models which use a refined mesh close to wall to resolve the near-wall flow details. The second method bridges the near-wall region and high Reynolds number region by wall functions. The wall function approach demands less computer resources than LRN models, although an amount of information is lost. A compromise can be achieved by implementing a two-layer model which presupposes division of the near-wall region into two sub-regions: for the part far from the wall, a k-ε model is adopted, whereas closing to the wall, the one-parameter k-l model is realized.

Many researchers have focused on investigations of the performance of the wall functions preferred by commercial CFD packages over the last few decades. Usually wall function methods assume a logarithmic velocity profile and are based on an analytical expression that is matched closely with experimental data (Launder and Spalding 1974). It is believed that wall functions can be a very useful tool in reducing the calculation cost for engineering applications as long as they are utilized appropriately (Mohammadi 2006). However, wall function methods often do not work well with complex flow situations, and early research works were conducted to improve their accuracy in complex flow situations such as separation and recirculating flows (Amano 1984, Ciofalo 1989).

Recent developments in wall function methods are mainly in two aspects: i) flow quantities are pre-prescribed by empirical expressions or expressions of simplified transport functions and ii) sub-grids are introduced into the first layer cells adjacent to the wall to resolve the flow details.

For the first kind improvement method, non-uniform distribution of the shear stress, the turbulent kinetic energy values or the viscous sub-layer thickness across the near-wall cells are assumed to improve the standard wall function (Chieng 1980, Johnson 1982, Amano 1984, Ciofallo 1989, Grotjans 1998). However, all the above attempts are still based on the log-law profile and it is well known that such a condition does not apply in flows with strong pressure gradients and separation (Launder 1984, 1988). Moreover, since a universal scale for turbulent buoyant thermal boundary layers has not been established yet, it is difficult to use empirical wall functions for such thermal phenomena (Hanjalic 2002).

In contrast to empirical expressions, Kalitzin *et al*. (2005) employed a database approach, to formulate a wall function methodology. Known from the standard wall function, Kalitzin et al. assumed the wall layer is universal for different types of flows. And the friction velocity (u_τ) is pre-calculated using a database. Through their study, this new wall function formulation was incorporated into three turbulence models (Spalart-Allmaras, *k-ω*, and υ^2-*f*) and evaluated for zero pressure gradient flow over a flat plate and a case of a streamwise pressure gradient over a flat plate. The test cases were designed to see how the proposed wall functions captured pressure gradient driven by separations and reattachments. A vast improvement was observed compared to the standard wall functions.

The UMIST-A (Unified Modelling through Integrated Sublayer Transport - an Analytical approach) method incorporates the analytical profiles of turbulent viscosity, temperature and velocity of viscous sublayer into turbulence model expressions (Craft 2004). This approach was designed to be applicable to flow regimes such as natural, mixed, or forced convection, steep changes of transport properties across the viscous sublayer, and thickening of the viscous sublayer in buoyancy-aided mixed convection. The computation time associated with using the model was one to two orders of magnitude less than a low-Reynolds model with comparable results.

As one of the subgrid approaches, the UMIST-N (Unified Modelling through Integrated Sublayer Transport - a Numerical approach) solves the simplified boundary layer transport equations that decouple the near-wall region from the whole boundary layer (Craft 2002). The UMIST-N divides the first-layer cells into a number of subgrids. By introduction of subgrids, the UMIST-N wall function is less sensitive to primary grid sizes normal to the wall than traditional methods. This model was tested for a 2-D fully developed channel flow and an axisymmetric impinging jet. The corresponding results were in good agreement with the LRN model simulations and better than those of the UMIST-A model.

Another wall function method developed by Walters *et al*. (2005) introduces a one-dimensional equation on the subgrids. The source terms in the first-layer cells are obtained by solving the one-dimensional equations of momentum and turbulence quantities to calculate wall shear stress (τ_ω) and turbulent production (G_P). To make the equations be closed, a linear profile of velocity along the height direction is assumed ranging from zero at the wall to interior grid value at the top of the subgrid. Turbulence model equations are also solved on the subgrids, assuming the convective terms are negligible. The test case for the new model is two-dimensional, zero pressure gradient flow over a flat plate. Grid sizes for the test case ranges from $y^+ = 1$ to $y^+ = 512$. Overall, the subgrid model produces better results for skin friction coefficients and velocity distributions.

The computation time is an order of magnitude less than the low-Re models and around 40% to 60% higher than the standard wall function method.

With the above discussions, the reason why there is still an interest in wall functions is due to the need to reduce computational costs, as well as to achieve better numerical stability and convergence speed. If it is possible to improve the predictions using wall functions, more problems of engineering interest can be solved effectively. Even with all the current near-wall treatments, certain improvements still require. Moreover, wall function methods' inability to accurately represent complex flows such as pressure gradient flow, acceleration around a curved surface, and stagnation points need to be overcome.

This study focuses on the derivation of a modified wall function formulation by means of combining inflow profiles and the realizable *k* -*ε* turbulence model. It will be shown that relatively simple adaptation of the modified wall function results in reproducing many features of

flows over rough surfaces, while retaining the computational efficiency high. The flow test cases chosen for the validation are horizontally homogenous atmospheric boundary layer (ABL) over rough surfaces and flows over a 6 m cube.

3. Modified wall function

Before presenting the modified wall function, some postulations are given firstly. Richards *et al.* (1993) made the following assumptions of 2D homogeneous ABL:
   1) The vertical velocity is zero.
   2) The pressure is constant in both the vertical and streamwise directions.
   3) The shear stress τ_ω is constant throughout the boundary layer

$$\tau_w = \mu_t \frac{\partial u_x}{\partial y} = \rho u_*^2 \tag{1}$$

Based on the above assumptions, the mean flow and realizable $k - \varepsilon$ turbulence functions can be re-arranged as

$$\frac{\partial}{\partial y}[\frac{1}{\rho}(\mu + \mu_t)\frac{\partial u_x}{\partial y}] = 0 \tag{2}$$

$$\frac{\partial}{\partial y}[\frac{1}{\rho}(\mu + \frac{\mu_t}{\sigma_k})\frac{\partial k}{\partial y}] + G_k - \varepsilon = 0 \tag{3}$$

$$\frac{\partial}{\partial y}[\frac{1}{\rho}(\mu + \frac{\mu_t}{\sigma_\varepsilon})\frac{\partial \varepsilon}{\partial y}] + C_1 S\varepsilon - C_2 \frac{\varepsilon^2}{k + \sqrt{\nu\varepsilon}} = 0 \tag{4}$$

The mean velocity at the first-layer cell centroid adjacent to the wall is

$$u_P = u_* \left(\frac{y_P + y_0}{y_0}\right)^\alpha \tag{5}$$

where the subscript *P* refers to the cell adjacent to the wall.
   Friction velocity u_* can be got from Eq. (5)

$$u_* = \sqrt{\tau_w/\rho} \tag{6}$$

Based on the local equilibrium assumption in the cells next to the wall, the turbulent kinetic energy K_P and dissipation rate ε_P are as follows

$$\begin{cases} k_P = \frac{3}{2}\left(u_*(\frac{y_P + y_0}{y_0})^\alpha \cdot 0.1(\frac{Y_b}{Y_G})^{-\alpha-0.05}\right)^2 \\ \varepsilon_P = C_\mu^{3/4}\frac{k_P^{3/2}}{y_P} \end{cases} \tag{7}$$

The friction velocity from Eq. (7) is

$$u_* = \frac{k_P^{1/2} \cdot (2/3)^{1/2} \cdot 10}{\left(\dfrac{y_P + y_0}{y_0}\right)^{\alpha} \cdot \left(\dfrac{Y_b}{Y_G}\right)^{-\alpha-0.05}} \tag{8}$$

Taking manipulations of Eqs. (6), (7) and (8), the shear stress at the wall τ_ω is given as

$$
\begin{aligned}
\tau_w &= \frac{\rho u_P}{\left(\dfrac{y_P + y_0}{y_0}\right)^{\alpha}} \cdot \frac{k_P^{1/2} \cdot (2/3)^{1/2} \cdot 10}{\left(\dfrac{y_P + y_0}{y_0}\right)^{\alpha} \cdot \left(\dfrac{Y_b}{Y_G}\right)^{-\alpha-0.05}} \\
&\approx \frac{\rho u_P}{\left(\dfrac{y_P + y_0}{y_0}\right)^{\alpha}} \cdot \frac{8.165 \cdot k_P^{1/2}}{\left(\dfrac{y_P + y_0}{y_0}\right)^{\alpha} \cdot \left(\dfrac{Y_b}{Y_G}\right)^{-\alpha-0.05}}
\end{aligned}
\tag{9}
$$

The mean velocity profile could be re-written as

$$u_x = \frac{8.165 \cdot k_P^{1/2}}{\left(\dfrac{y_P + y_0}{y_0}\right)^{\alpha} \cdot \left(\dfrac{Y_b}{Y_G}\right)^{-\alpha-0.05}} \left(\frac{y + y_0}{y_0}\right)^{\alpha} \tag{10}$$

So the normal derivative for mean wind velocity profile function is given by

$$\frac{\partial u_x}{\partial y} = \frac{8.165 \cdot k_P^{1/2}}{\left(\dfrac{y_P + y_0}{y_0}\right)^{\alpha} \cdot \left(\dfrac{Y_b}{Y_G}\right)^{-\alpha-0.05}} \cdot \left(\frac{y + y_0}{y_0}\right)^{\alpha-1} \frac{\alpha}{y_0} \tag{11}$$

The production of turbulent kinetic energy G_P in the wall-adjacent cell is

$$
\begin{aligned}
G_P &= \tau_w \frac{\partial u}{\partial y} = \frac{\tau_w^2 \left(\dfrac{y + y_0}{y_0}\right)^{\alpha-1} \dfrac{\alpha}{y_0}}{\dfrac{8.165 \cdot k_P^{1/2}}{\left(\dfrac{y_P + y_0}{y_0}\right)^{\alpha} \cdot \left(\dfrac{Y_b}{Y_G}\right)^{-\alpha-0.05}}} \\
&= \frac{\tau_w^2 \left(\dfrac{y + y_0}{y_0}\right)^{\alpha-1} \dfrac{\alpha}{y_0} \left(\dfrac{y_P + y_0}{y_0}\right)^{\alpha} \cdot \left(\dfrac{Y_b}{Y_G}\right)^{-\alpha-0.05}}{8.165 \cdot k_P^{1/2}}.
\end{aligned}
\tag{12}
$$

Distinguished from the standard wall function method, hereby the evaluation of turbulence production across the first-layer cell adjacent the wall is given as follows

$$\overline{G_P} = \frac{1}{2y_P} \int_{y_0}^{2y_P} G_P \, \mathrm{d}y = \frac{1}{2y_P} \int_{y_0}^{2y_P} \tau_w \frac{\partial u}{\partial y} \, \mathrm{d}y$$

$$= \frac{1}{2y_P} \frac{\left[\left(\dfrac{2y_P + y_0}{y_0}\right)^\alpha - 2^\alpha \right] \tau_w^2 \left(\dfrac{y_P + y_0}{y_0}\right)^\alpha \cdot \left(\dfrac{Y_b}{Y_G}\right)^{-\alpha - 0.05}}{8.165 \cdot k_P^{1/2}} \qquad (13)$$

where y_0 is the aerodynamic roughness height, y_P is the half length of the first-layer cell.

The dissipation rate ε in the cells adjacent to the wall falls into two different parts: the fully turbulent region and the viscosity affected region. It is usually to set ε constant without solving it as follows

$$\varepsilon_P = C_\mu^{3/4} \frac{k_P^{3/2}}{y} + \frac{2\mu k_P}{\rho y^2} \qquad (14)$$

The evaluation of dissipation rate across the first-layer cell is also assumed to be separated into two parts: flow at $y \in [y_0, y_P]$ is viscosity affected part and flow at $y \in [y_P, 2y_P]$ is fully turbulent part. So the dissipation rate ε across the first-layer cells next to the wall is expressed as follows

$$\overline{\varepsilon_P} = \frac{1}{2y_P - y_P} \int_{y_P}^{2y_P} C_\mu^{3/4} \frac{k_P^{3/2}}{y} \mathrm{d}y + \frac{1}{y_P - y_0} \int_{y_0}^{y_P} \frac{2\mu k_P}{\rho y^2} \mathrm{d}y$$

$$= \frac{\ln 2 \cdot C_\mu^{3/4} k_P^{3/2}}{y_P} + \frac{2\mu k_P}{\rho y_P y_0} \qquad (15)$$

Based on the above detailed derivation, the modified wall function can be expressed as follows

$$\begin{cases} \overline{G_P} = \dfrac{1}{2y_P} \dfrac{\left[\left(\dfrac{2y_P + y_0}{y_0}\right)^\alpha - 2^\alpha \right] \tau_w^2 \left(\dfrac{y_P + y_0}{y_0}\right)^\alpha \cdot \left(\dfrac{Y_b}{Y_G}\right)^{-\alpha - 0.05}}{8.165 \cdot k_P^{1/2}} \\[3em] \overline{\varepsilon_P} = \dfrac{\ln 2 \cdot C_\mu^{3/4} k_P^{3/2}}{y_P} + \dfrac{2\mu k_P}{\rho y_P y_0} \\[2em] \tau_w = \dfrac{\rho u_P}{\left(\dfrac{y_P + y_0}{y_0}\right)^\alpha} \cdot \dfrac{8.165 \cdot k_P^{1/2}}{\left(\dfrac{y_P + y_0}{y_0}\right)^\alpha \cdot \left(\dfrac{Y_b}{Y_G}\right)^{-\alpha - 0.05}} \end{cases} \qquad (16)$$

The modified wall function differs from the standard wall function such as that it considers the upstream inflow distributions and also controls the turbulent kinetic energy generation and dissipation. Since, the modified wall function can keep the flow stable and does not suffer from the convergence problems encountered by the low Reynolds number models. The coding of the modified wall function will be validated in the following sections by modelling boundary layer flow over rough wall and flow around a 6m cube located in the ABL.

4. Turbulence modelling and boundary conditions

4.1 Nonlinear eddy viscosity model

For the k-ε variant models, Reynolds stresses are modelled by the linear constitutive expression

$$-\rho\overline{u'v'} = C_\mu \rho U_{scale}^2 T_{scale} S_{ij} - \frac{2}{3}\rho k \sigma_{ij} \tag{17}$$

where $U_{scale} = \sqrt{k}$ is the turbulent velocity scale, $T_{scale} = k/\varepsilon$ is the turbulent time scale and C_μ is a model constant (= 0.09). The turbulent viscosity μ_t can be expressed by

$$\mu_t = C_\mu \rho k^2 / \varepsilon \tag{18}$$

Since the $k - \varepsilon$ models do not take into account the anisotropic characteristics of the Reynolds stresses. This shortcoming can be overcome to some extent by introducing a nonlinear eddy viscosity assumption as follows (Craft 2001)

$$\rho u_i' u_j' = \underbrace{-\mu_t S_{ij} + 2/3\delta_{ij}k}_{\text{I}} + \underbrace{C_1 \mu_t \frac{k}{\varepsilon}(\Omega_{ik}S_{kj} + \Omega_{jk}S_{ki})}_{\text{II}}$$
$$+ \underbrace{C_2 \mu_t \frac{k}{\varepsilon}(S_{ik}S_{kj} - 1/3 S_{kl}S_{kl}\delta_{ij})}_{\text{III}} + \underbrace{C_3 \mu_t \frac{k}{\varepsilon}(\Omega_{ik}\Omega_{jk} - 1/3\Omega_{lk}\Omega_{lk}\delta_{ij})}_{\text{IV}} \tag{19}$$

where $S_{ij} = \partial u_i/\partial x_j + \partial x_j/\partial x_i$, $\Omega_{ij} = \partial u_i/\partial x_j - \partial x_j/\partial x_i$. Nonlinear terms in II, III and IV parts are expressed by strain and rotation tensors (Pope 1975, Speziale 1991). To keep the components of the anisotropic tensors satisfy the realizable condition, the tuning function $f_M(M)$ can be introduced

$$f_M(M) = \frac{1}{1 + 0.01M^2} \tag{20}$$

where $M = \max(S, \Omega)$. We also introduce the tuning function $f_M(M)$ into C_1, C_2, C_3 and C_μ to make sure that the diagonal components of the Reynolds stress tensors should be nonnegative, which is also a mathematic restriction.

The nonlinear eddy viscosity model can be summarized as

$$\begin{cases} \rho u_i' u_j' = -\mu_t S_{ij} + 2/3\delta_{ij}k + C_1 \mu_t \dfrac{k}{\varepsilon}(\Omega_{ik}S_{kj} + \Omega_{jk}S_{ki}) \\[2mm] \qquad + C_2 \mu_t \dfrac{k}{\varepsilon}\left(S_{ik}S_{kj} - \dfrac{1}{3}S_{kl}S_{lk}\delta_{ij}\right) + C_3 \mu_t \dfrac{k}{\varepsilon}\left(\Omega_{ik}\Omega_{kj} - \dfrac{1}{3}\Omega_{kl}\Omega_{lk}\delta_{ij}\right) \\[2mm] C_1 = 0.4 f_M(M), \quad C_2 = 0, \quad C_3 = -0.13 f_M(M), \\[2mm] C_\mu = \min\left(0.09, 0.3 f_M(M)\right), \quad f_M(M) = \dfrac{1}{1 + 0.01M^2} \end{cases} \tag{21}$$

4.2 Numerical schemes

The set of N-S equations are solved using the finite volume techniques over a non-stagger discretization scheme. And structured grid is adopted. SIMPLEC (semi-implicit method for pressure-linked equations consistent) is used to solve the velocity–pressure coupling term. Diffusion terms and convective terms are discretized by second-order UPWIND scheme. All the simulations have been carried out by a steady iterative algorithm. The modified wall function has been implemented with the realizable k -ε model based on FLUENT platform. For further comparisons, flow predictions have also been obtained using the standard wall function, while full-scale measurement data are available for validation of the simulated results for the case of flows around a 6 m cube.

4.3 Boundary conditions

Wind velocity varies with terrain roughness near the earth ground, such as sands, trees and buildings etc. The terrain roughness friction force influences the atmospheric boundary layer from the ground to the gradient height. Terrain roughness causes a gradual decrease in wind speed and wind velocity profile changes with different terrain roughness categories. For a fully developed boundary layer, the velocity profile can be represented by a power law or a logarithmic law.

The following power law of mean wind velocity profile is adopted in this paper

$$u_y = u_{y_0} \left(\frac{y}{y_0} \right)^\alpha \tag{22}$$

where u_y (m/s) is the mean wind velocity at height y (m), u_{y_0} (m/s) is the friction velocity at height y_0 (m) which is the aerodynamic roughness height. It is assumed that the velocity at height $y = y_0$ is equal to u_*. And α is the power law exponent which is a parameter depending on terrain roughness conditions.

According to the recommendation of AIJ (Architectural Institute of Japan), the turbulence intensity I is defined as

$$I = \begin{cases} 0.1 \left(\dfrac{y}{Y_G} \right)^{-\alpha-0.05} & , Y_b < y <= Y_G; \\ 0.1 \left(\dfrac{Y_b}{Y_G} \right)^{-\alpha-0.05} & , y <= Y_b. \end{cases} \tag{23}$$

where y is the height along the fetch; Y_b, Y_G and α are parameters determined by terrain roughness conditions (AIJ 2004).

The turbulent kinetic energy k at the inlet condition is defined by turbulence intensity I as follows

$$k = \frac{3}{2}(u_y \cdot I)^2 \tag{24}$$

The dissipation rate ε can be determined by k and the turbulence length scale L, and the relationship is

$$\varepsilon = C_\mu^{3/4} \frac{k^{3/2}}{L} \tag{25}$$

where C_μ is an empirical constant specified in the turbulence model (0.09 is adopted in this study).

Turbulence scale L is defined independent of the terrain conditions of the site as

$$L = \begin{cases} 100\left(\dfrac{y}{30}\right)^{0.5}, & 30 < y <= Y_G; \\ 100, & y <= 30m. \end{cases} \qquad (26)$$

In summary, the inlet boundary condition of turbulent kinetic energy k and dissipation rate ε are listed below

$$\begin{cases} k(x) = \dfrac{3}{2}\left(u_0(\dfrac{y+y_0}{y_0})^\alpha \cdot I\right)^2 \\[2mm] \varepsilon(x) = C_\mu^{3/4}\dfrac{k^{3/2}}{L} \\[2mm] I = \begin{cases} 0.1\left(\dfrac{y}{Y_G}\right)^{-\alpha-0.05}, & Y_b < y <= Y_G; \\[2mm] 0.1\left(\dfrac{Y_b}{Y_G}\right)^{-\alpha-0.05}, & y <= Y_b. \end{cases} \\[4mm] L = \begin{cases} 100\left(\dfrac{y}{30}\right)^{0.5}, & 30 < y <= Y_G; \\ 100, & y <= 30m. \end{cases} \end{cases} \qquad (27)$$

The shear stress τ_ω, turbulent kinetic energy production $\overline{G_P}$ and dissipation rate $\overline{\varepsilon_P}$ appropriate to the modified wall function are applied in the cells next to the wall (Fig. 1). The boundary conditions of top and bilateral boundaries are set as slip boundary conditions, which are expressed as

$$\begin{cases} u_y = 0, \ \dfrac{\partial}{\partial x}(u_x, u_z, k, \varepsilon) = 0, \\[3mm] u_z = 0, \ \dfrac{\partial}{\partial x}(u_x, u_y, k, \varepsilon) = 0. \end{cases} \qquad (28)$$

The outflow face is assumed as fully developed outflow boundary condition which can be expressed as

$$\frac{\partial}{\partial x}(u_x, u_y, u_z, k, \varepsilon) = 0 \qquad (29)$$

5. Horizontally homogenous ABL

The following case is considered in this study to examine the performance of the modified wall function. Horizontally homogenous ABL flow is modelled to obtain self-sustainable ABL profiles of mean wind speed and turbulence quantities by Fluent (2006). The whole domain is set as 246 m (Length)×50 m (Height)×100 m (Width), which allows inflow quantities to dissipate and to ensure a fully developed flow towards the outlet.

The grid scheme is shown in Fig. 2. The mesh scheme used for the horizontally homogenous ABL flow includes 50 nodes normal to the wall (y-direction). The first-layer cell height is dy_P/H = 10^{-4} (H for the whole height of the fetch), corresponding to local Reynolds number $Re_x > 30$ ($Re_x = \rho u y_P/\mu$), which is suitable for wall function. To avoid high aspect ratio between the cells, stretching ratio of the two adjacent cells is 1.15. For the meshes along the fetch (x-direction), 100 nodes are adopted and the stretching ratio is 1.2. The number of nodes across the fetch (z-direction) is relatively small as there is no flow quantity variation.
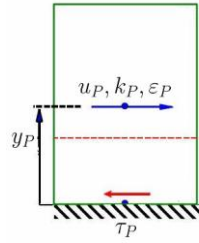
Fig. 1 Flow quantities in the near-wall cells
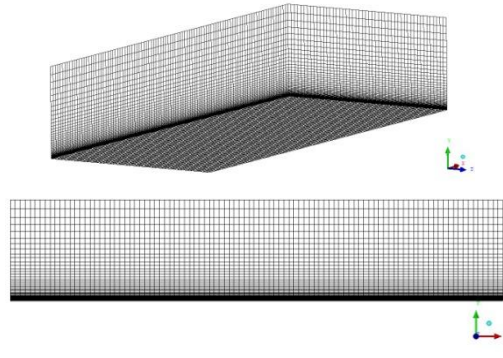
Fig. 2 Mesh schematic of the empty fetch

Profiles of x-component (longitudinal) mean velocity u_x, turbulent kinetic energy k and dissipation rate ε values by Standard Wall Function (SWF) are presented in Figs. 3(a), 3(b) and 3(c), respectively. It is noted that the flow quantity profiles of six different locations along the fetch cannot maintain well, especially for k and ε. The results of mean velocity u_x are acceptable, except for several layer cells adjacent to the wall. The maximum errors are beyond 100% compared to the inlet profile. It is evident that the standard wall function method results in an internal boundary layer (IBL) over the whole fetch. Obviously, the IBL will cause incorrect flow fields around structures.

The modified wall function is incorporated into Fluent to model horizontal homogenous ABL flow. Fig. 4(a) shows the mean velocity profiles of six different positions along the fetch. In the rough ABL with h/D = 10^{-4} (D: fetch height), it is clear that the realizable k-ε model with the modified wall function reproduces the log-law distribution for fully rough wall flows. Since the wall function is quite insensitive to near-wall grid size, discrepancies between the profiles are

hardly seen. The maximum difference of non-dimensional mean wind velocity is around 1.57%, which occurs in the first layer cells adjacent to the wall.
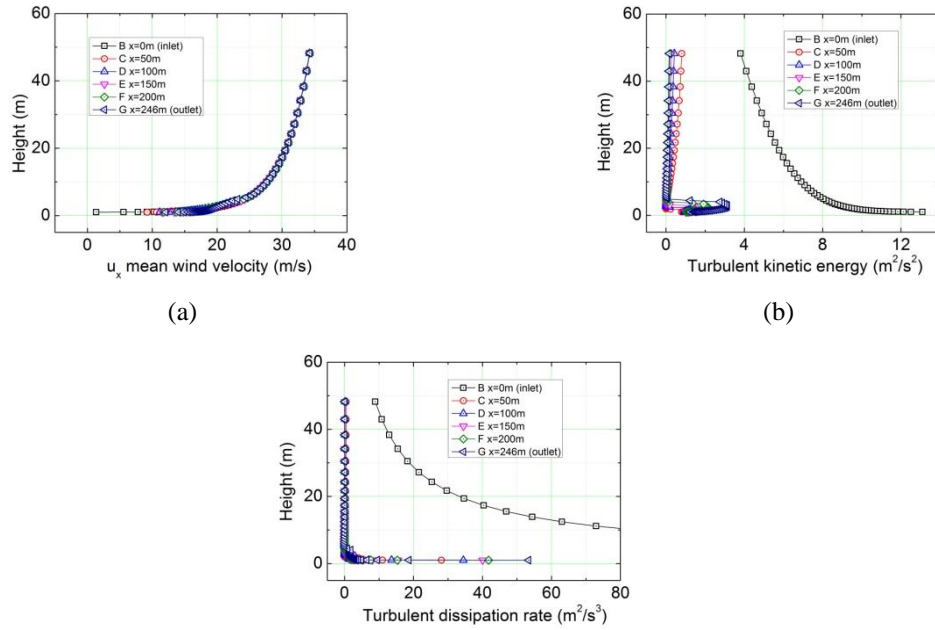

(a)

(b)

Fig. 3 (a) Profiles of longitudinal mean velocity, (b) profiles of TKE and (c) profiles of dissipation rate
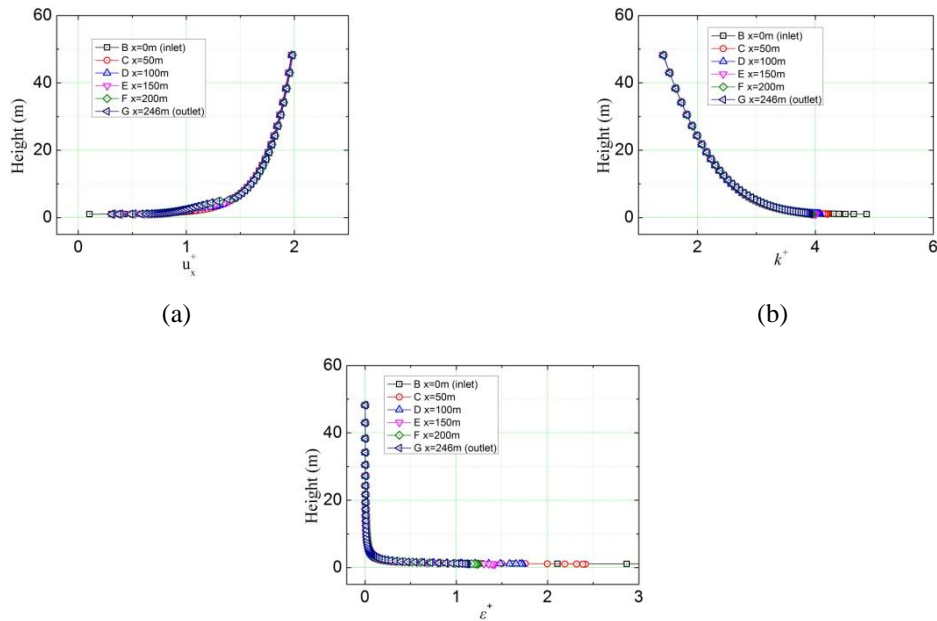

(a)

(b)

Fig. 4 (a) Profiles of longitudinal mean velocity, (b) profiles of TKE and (c) profiles of dissipation rate

Fig. 4(b) shows the turbulent kinetic energy (TKE) *k* profiles of six different positions along the fetch. In the case of a rough wall, similar to the mean velocity profiles, the TKE distributions along the height maintain quite well. For $y^+<0.12$, especially in the first three wall-adjacent cells, the non-dimensional TKE value changes from 4.870 to 3.912. The maximum difference is around 19.7%. With increase of the height, the discrepancies become small and the six profiles show good consistency. The spike of the TKE profile occurs in the first layer cell adjacent to the wall. This, however, is one feature of the wall function approach (Walshe 2003).

Fig. 4(c) shows the dissipation rate ε distribution of six different positions along the fetch. Similar to the profiles of TKE, the ε distributions along the height maintain quite well. The maximum discrepancy is about 16.7% which occurs in the second wall-adjacent cells. And the non-dimensional ε value changes from 2.867 to 2.388.

Based on the u_x, *k* and ε distribution results, it can be concluded that the profiles of turbulence kinetic viscosity ν_t ($C_\mu \dfrac{k^2}{\varepsilon}$) and Reynolds shear stress $-u'v'$ ($\nu_t \dfrac{\partial u_x}{\partial y}$) show good consistency.

Overall, it is observed that the realizable *k*-ε model combined with the modified wall function yield perfectly matched profiles at six different positions along the whole fetch.
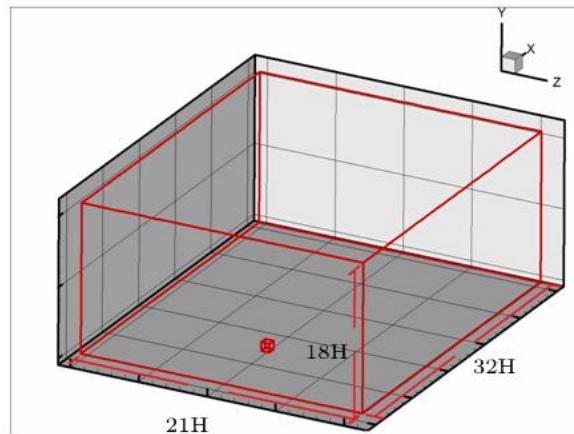

Fig. 5 Schematic of flow around 6 m cube

6. Flow around a 6 m Cube at perpendicular incident flow

Three-dimensional numerical study of turbulent flow over a 6 m cube mounted on the ABL is performed by the realizable *k*-ε turbulence model combined with the modified wall function (MWF) and the standard wall function (SWF). A 6 m cube mounted on the ABL is considered here to test the modified wall function's abilities to generate accurate results of reattached and separated flows and associated surface pressure distributions. The 6 m cube at a normal orientation to the incident wind with the constructed computational domain is shown in Fig. 5. Further

representations of the computational domain and mesh arrangements can be seen in Figs. 6(a) and 6(b), respectively.

Reynolds number based on the incident wind velocity and the height of the 6 m cube model is around 10^7. To resolve the flow field around the bluff body, the first-layer cell near the cube surface is set as $0.015 H_c$, which is appropriate for MWF application. The cells are non-uniformly distributed and the stretching ratio is 1.12 along the surfaces. 32 grids are placed on the windward, roof and leeward surfaces of the cube (z-direction). And 40 grids are located along the lateral faces of the cube (y-direction). 30 grids with stretching ratio 1.2 are placed in the wake zone of the computational domain.

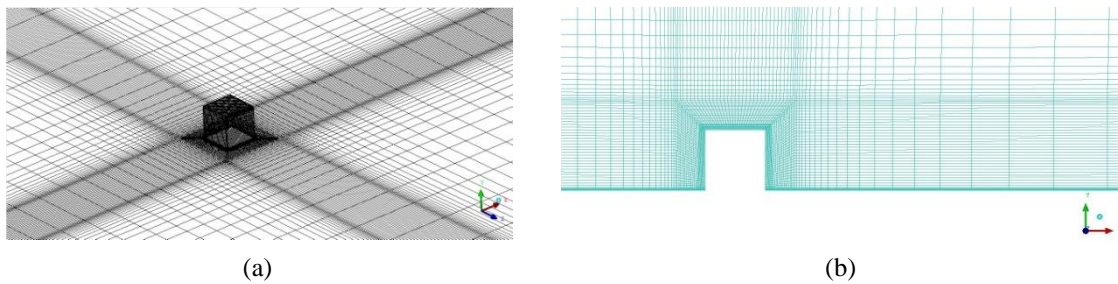(a)   (b)

Fig. 6 (a) The grid for numerical models and (b) the grid for numerical models

Moreover, the TKE generation and turbulence viscosity predictions by the MWF and SWF models are plotted in Figs. 7 and 8. It is clear that there exists a TKE generation spike at the stagnation area because of wind flow impinging (Figs. 7(a), 7(b), 8(a) and 8(b)). The MWF model significantly reduces the turbulent kinetic energy in the impinging region (Figs. 7(a) and 7(b)). The over-predicted turbulent viscosity results in the prediction of small separation bubble but large and downstream arch vortex prediction. From Figs. 7(e) and 8(e), it is noted that the MWF predicts smaller value of TKE generation and turbulent viscosity than SWF model, which keeps the separation bubble over the leading edge and leeward exist. The turbulent viscosity in the wake regions predicted by the MWF model is smaller than those predicted by the SWF model, and they are closer to the real values of fully developed turbulent flows. However, the turbulence predicted by SWF in the wake region (where rotation vorticity larger than strain rate) is larger than that of MWF model (Figs. 7(c) and 8(c)). This concludes that the SWF model would under-predict the value of drag distributions.

Pressure coefficient is an appropriate form to illustrate the pressure distribution which is calculated by dividing the dynamic pressure determined at the height of 6m, i.e., obtained from 0.5 $\rho u_{H=6}^2$. Fig. 9 shows a comparison of the centreline pressure distributions from both numerical simulations and full-scale measurement results (Castro and Robins 1977). Although the distributions of the three sets of results are similar, the numerical results based on the modified wall function are much closer to the experimental data. The results show that the maximum mean pressure coefficients on the windward wall range from 0.59 to 0.85 where they generally occur at about three-quarters of the way up the wall. The results also show a local minimum at about one-quarter height along the windward surface (Easom 2000). From Fig. 9, it is believed that the realizable k-ε model with the modified wall function yield similar results to the experimental ones and better results than the standard wall function.
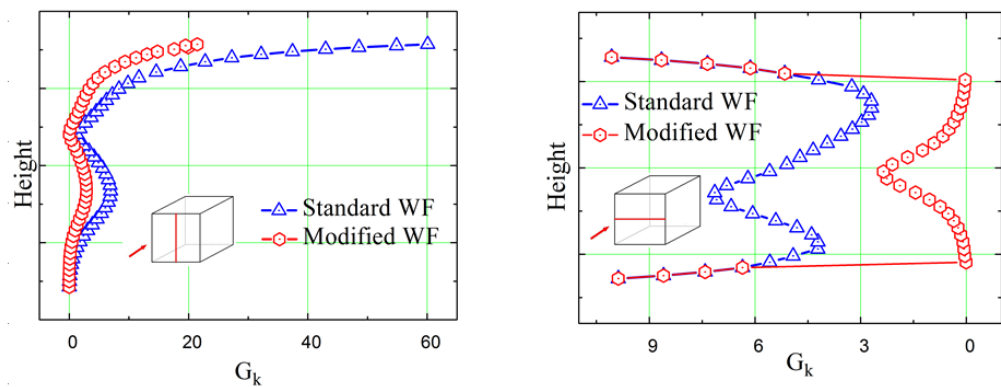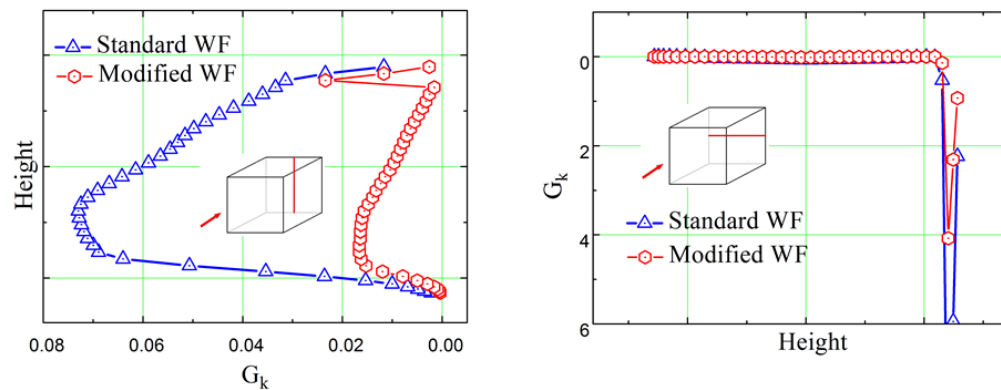
Fig. 7 (a) and (b)TKE generation on windward surface
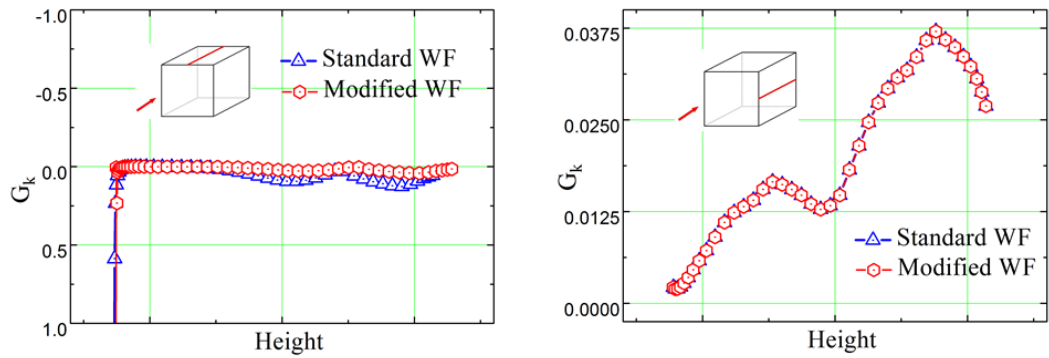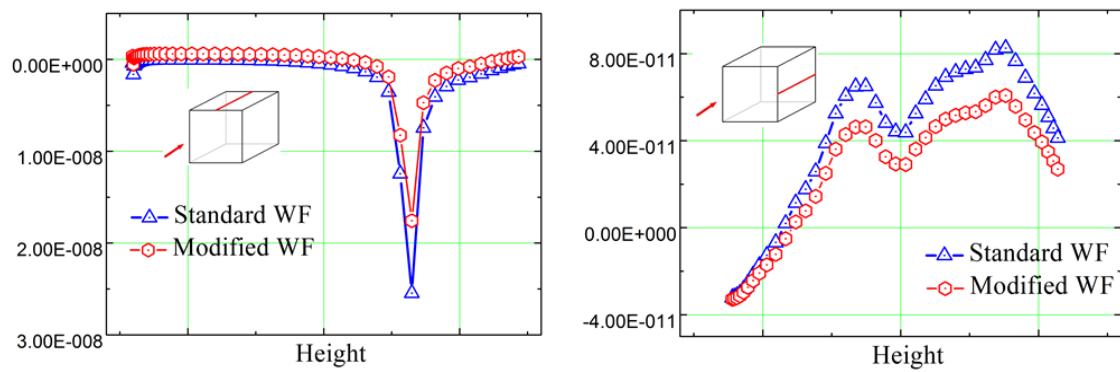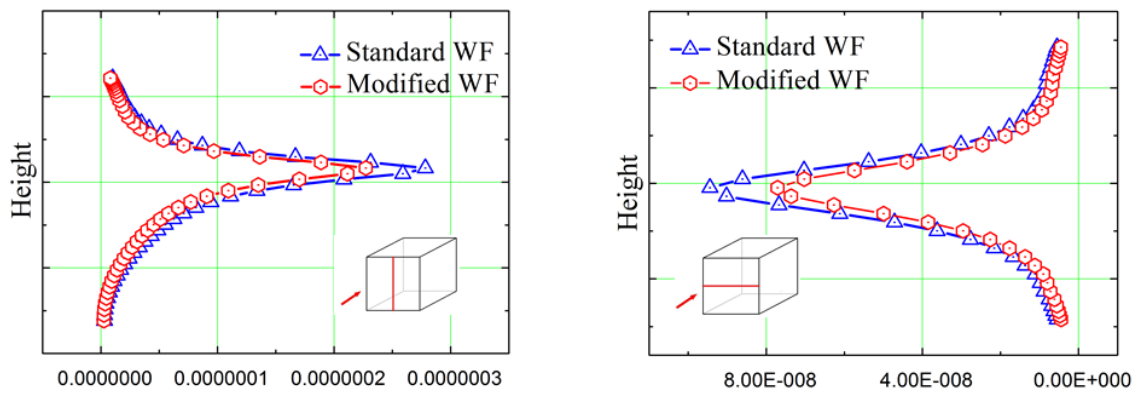

Fig. 7 (c) and (d) TKE generation on leeward surface

Fig. 7 (e) and (f) TKE generation on roof and lateral surfaces

Fig. 8 (a) and (b) turbulence viscosity on windward surface

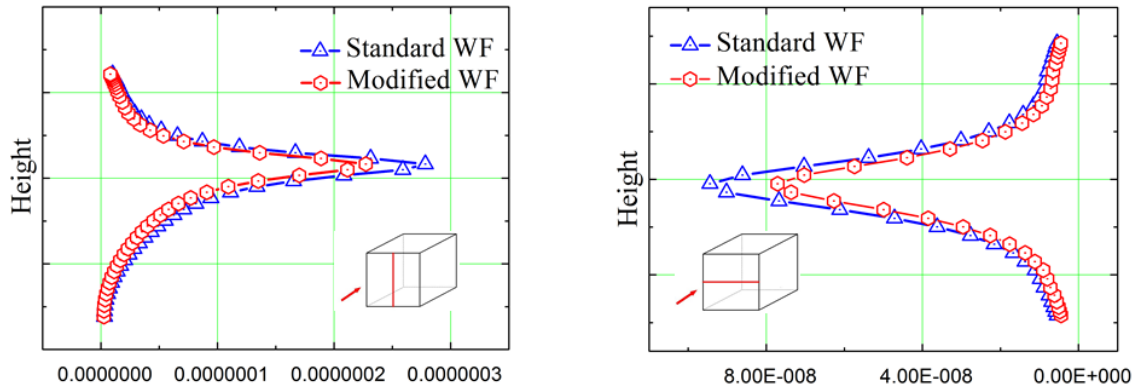Fig. 8 (c) and (d) turbulence viscosity on leeward surface

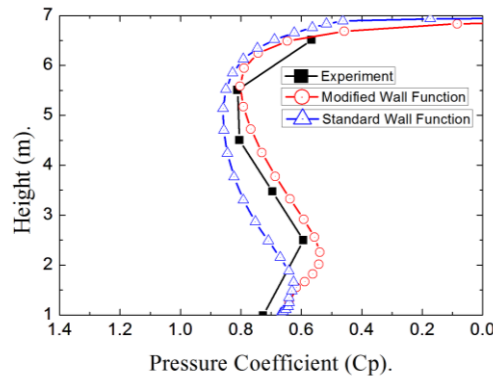Fig. 8 (e) and (f) turbulence viscosity on roof and lateral surfaces

Fig. 9 Windward centreline pressure distributions

7. Conclusions

A numerical study of the mean flow field and turbulence structure over a rough plane and a 6 m cube mounted in three-dimensional rough-wall turbulent boundary layers have been carried out and the distributions of selected flow and surface pressure quantities were presented and discussed.

The results from the case of flow over rough wall show that the modified wall function, derived from streamwise mean velocity and turbulence quantities profiles, yields perfect homogeneous equilibrium boundary layer. Additionally, the only requirement for the modified wall function is that the first-layer cell centroid should be located within the local Reynolds number. It is realized that the inlet profiles, turbulence model, near-wall treatment and mesh scheme have influences on the horizontal inhomogeneity in an empty fetch without obstacle models present.

Simulations of mean pressure distributions on the windward surface of a 6 m cube have been compared with available full-scale measurements. The modified wall function and the standard wall function are all adopted to predict the TKE generation, turbulence viscosity, flow fields and the pressure distributions based on the realizable k-ε model. The major differences between the simulated results appear to be related to the use of different near-wall treatment methods. For the case of the incident flow normal to the windward surface of the cube, it is found that the results predicted by the realizable k-ε model combined with the modified wall function are much closer to the full-scale measurement data and supress the turbulence over-prediction, illustrating the effectiveness of the modified wall function.

The results of the two cases study have shown significant improvements of the modified wall function over the standard wall function treatments.

Acknowledgements

References

Architectural Institute of Japan (2004), *AIJ recommendations for loads on buildings Tokyo*, Japan: Architectural Institute of Japan.

Blocken, B. and Carmeliet, J. (2006), "The influence of the wind-blocking effect by a building on its wind-driven rain exposure", *J. Wind Eng. Ind. Aerod.*, **94**(2), 101-127.

Castro, I.P. and Robins, A.G. (1977), "The flow around a surface-mounted cube in uniform and turbulent streams", *J. Fluid Mech.*, **79**(2), 307-335.

Craft, T.J. and Launder, B.E. (2001), "On the spreading mechanism of the three-dimensional turbulent wall jet", *J. Fluid Mech.*, **435**, 305-326.

Easom, G. (2000), *Improved turbulence models for computational wind engineering*, Ph.D Thesis, University of Nottingham.

Franke, J., Hirsch, C., Jensen, A.G., Krüs, H.W., Schatzmann, M., Westbury, P.S., Miles, S.D., Wisse, J.A. and Wright, N.G. (2004), "Recommendations on the use of CFD in wind engineering", *Proceedings of the International Conference on Urban Wind Engineering and Building Aerodynamics*, (Ed. van Beeck JPAJ), COST Action C14, Impact of Wind and Storm on City Life Built Environment, von Karman Institute, Sint-Genesius-Rode, Belgium, May, 5 -7.

Franke, J. and Frank, W. (2005), "Numerical simulation of the flow across an asymmetric street intersection", (Eds. Náprstek, J. and Fischer, C.), *Proceedings of the 4EACWE*, Prague, Czech Republic, July 11-15.

Hargreaves, D.M. and Wright, N.G. (2007), "On the use of the k-ε model in commercial CFD software to model the neutral atmospheric boundary layer", *J. Wind Eng. Ind. Aerod.*, **95**, 355-369.

Mathews, E.H. (1987), "Prediction of the wind-generated pressure distribution around buildings", *J. Wind Eng. Ind. Aerod.*, **25**, 219-228.

Miles, S. and Westbury, P. (2003), *Practical tools for wind engineering in the built environment*, QNET-CFD Network Newsletter.

Murakami, S. (1998), "Overview of turbulence models applied in CWE-1997", *J. Wind Eng. Ind. Aerod.*, **74-76**, 1-24.

Murakami, S. (2002), "Setting the scene: CFD and symposium overview", *Wind Struct.*, **5**(2-4), 83-88.

Pope, S.B. (1975), "A more general eddy-viscosity hypothesis", *J. Fluid Mech.*, **72**, 331-340

Richards, P.J. and Hoxey, R.P. (1993), "Appropriate boundary conditions for computational wind engineering models using the *k-ε* model", *J. Wind Eng. Ind. Aerod.*, **46-47**, 145-153.

Riddle, A., Carruthers, D., Sharpe, A., McHugh, C. and Stocker, J. (2004), "Comparisons between FLUENT and ADMS for atmospheric dispersion modeling", *Atmos. Environ.*, **38**(7), 1029-1038.

Speziale, C.G., Sarkar S. and Gatski T.B. (1991), "Modelling the pressure-strain correlation of turbulence: an invariant dynamical systems approach", *J. Fluid Mech.*, **227**, 245-272

Walshe, J. (2003), *CFD modelling of wind flow over complex and rough terrain*, Ph.D. Thesis, University of Loughborough.

Yang, W. (2004), *Numerical study on structural wind loads and response based on RANS technique*, Ph.D Thesis, Tongji University.

Yang, W., Quan, Y., Jin, X., Tamura, Y. and Gu, M. (2008), "Influences of equilibrium atmosphere boundary layer and turbulence parameters on wind load distributions of low-rise buildings", *J. Wind Eng. Ind. Aerod.*, **96**(10-11), 2080-2092.

CC